Design of New Materials for Methane Storage

Tina Düren,† Lev Sarkisov,† Omar M. Yaghi,‡ and Randall Q. Snurr*,†

Department of Chemical Engineering, Northwestern University, Evanston, Illinois 60208, and Department of Chemistry, University of Michigan, Ann Arbor, Michigan 48109

Received August 21, 2003. In Final Form: November 13, 2003

One of the strategic goals of the modern automobile manufacturing industry is to replace gasoline and diesel with alternative fuels such as natural gas. In this report, we elucidate the desired characteristics of an optimal adsorbent for gas storage. The U.S. Department of Energy has outlined several requirements that adsorbents must fulfill for natural gas to become economically viable, with a key criterion being the amount adsorbed at 35 bar. We explore the adsorption characteristics of novel metal−organic materials (IRMOFs and molecular squares) and contrast them with the characteristics of two zeolites, MCM-41, and different carbon nanotubes. Using molecular simulations, we uncover the complex interplay of the factors influencing methane adsorption, especially the surface area, the capacity or free volume, the strength of the energetic interaction, and the pore size distribution. We also explain the extraordinary adsorption properties of IRMOF materials and propose new, not yet synthesized IRMOF structures with adsorption characteristics that are predicted to exceed the best experimental results to date by up to 36%.

Introduction

According to U.S. Department of Energy (DOE), alternative fuels must be substantially nonpetroleum, provide energy security and environmental benefits, and substitute for conventional fuels such as gasoline and diesel.[1] Natural gas, which consists mainly of methane, fits this definition and is widely available in many countries. In current practice, natural gas is mainly stored as compressed natural gas (CNG) at 207 bar in pressure vessels requiring an expensive multistage compression. An attractive alternative to CNG is adsorbed natural gas (ANG), where the gas is stored as an adsorbed phase in a porous solid at a lower pressure. In 1993, the DOE defined the storage target at 35 bar as 150 v/v, that is, the volume of gas adsorbed at standard temperature and pressure (STP; 298 K, 1 atm) per volume of the storage vessel.[2] More recently, this storage target was revised to 180 v/v so that the energy density of ANG becomes comparable to that of CNG.[3] A review of porous adsorbents for vehicular applications[4] points out that the adsorbents with the highest methane capacity are activated carbons where storage values up to 200 v/v have been reported.[2] In a recent paper, Eddaoudi et al.[5] report that a new material, IRMOF-6, exhibits an exceptionally high capacity for methane storage. IRMOF-6 is one member of a family of crystalline materials formed from metal−oxide clusters bridged by functionalized organic links and known as isoreticular metal−organic frameworks (IRMOFs). An important advantage of IRMOF materials over activated carbons is their crystallinity and consistency of properties from sample to sample. In addition, because of the building-block synthesis method, one can easily develop a strategy for designing and tailoring IRMOFs for particular applications.

The aim of this paper is twofold. First, we use molecular simulations to identify important factors that influence methane adsorption and explain why IRMOF-6 shows such a high uptake of methane. We do this by comparing the simulated methane uptake and other properties of IRMOF-6 with those of different adsorbents such as IRMOF-1 and IRMOF-14 (see Figure 1b), molecular squares (another example of metal−organic materials), two zeolites (silicalite and faujasite), an MCM-41 material, and different carbon nanotubes. Second, we propose two not yet synthesized IRMOF materials that should show an even higher uptake of methane, demonstrating how molecular simulations can complement and guide experimental efforts to design new materials by screening possible candidates.

IRMOF materials, first synthesized by Yaghi and coworkers,[5−7] are prepared in a self-assembly process that is shown schematically in Figure 1a. Each oxide-centered Zn_4O tetrahedron is linked by six carboxylate molecules resulting in an extended three-dimensional cubic porous network. By using different linkers, frameworks with different cavity sizes and different chemical functionalities are created. The linkers are oriented in a paddlewheel fashion so that each material has two different cavities, one in which all linker molecules are pointing in and one in which all are pointing out. In IRMOF-6, for example, the sizes of the cavities are 9.1 and 14.5 Å, and in IRMOF-14 they are 14.7 and 20.1 Å. The three-dimensional networks are very open (e.g., the free volume of IRMOF-14 is 85%), and some of these materials, among them IRMOF-14, have the lowest density so far reported for crystalline materials.[5]

Molecular squares are related materials, but instead of forming three-dimensional networks, they occur as discrete molecules. The corners of molecular squares consist of rhenium coordinated complexes ($[Re(CO)_3Cl]$) linked by different organic molecules.[8] We included the crystalline pyrazine[9] and bipyridine molecular squares[9,10] as well as

* To whom correspondence should be addressed. Phone: 1-847-467-2977. Fax: 1-847-467-1018. E-mail: snurr@northwestern.edu.
† Northwestern University.
‡ University of Michigan.

(1) U.S. Energy Policy Act of 1992 (EPAct).
(2) Wegrzyn, J.; Gurevich, M. *Appl. Energy* **1996**, *55*, 71.
(3) Burchell, T.; Rogers, M. *SAE Tech. Pap. Ser.* **2000**, 2000-01-2205.
(4) Menon, V. C.; Komarneni, S. *J. Porous Mater.* **1998**, *5*, 43.
(5) Eddaoudi, M.; Kim, J.; Rosi, N.; Vodak, D.; Wachter, J.; O'Keeffe, M.; Yaghi, O. M. *Science* **2002**, *295*, 469.
(6) Li, H.; Eddaoudi, M.; O'Keeffe, M.; Yaghi, O. M. *Nature* **1999**, *402*, 276.
(7) Chen, B.; Eddaoudi, M.; Hyde, S. T.; O'Keeffe, M.; Yaghi, O. M. *Science* **2001**, *291*, 1021.
(8) Dinolfo, P. H.; Hupp, J. T. *Chem. Mater.* **2001**, *13*, 3113.
(9) Slone, R. V.; Hupp, J. T.; Stern, C. L.; Albrecht-Schmitt, T. E. *Inorg. Chem.* **1996**, *35*, 4096.
(10) Bélanger, S.; Hupp, J. T.; Stern, C. L.; Slone, R. V.; Watson, D. F.; Carell, T. G. *J. Am. Chem. Soc.* **1999**, *121*, 557.

10.1021/la0355500 CCC: $27.50
Published on Web 03/02/2004

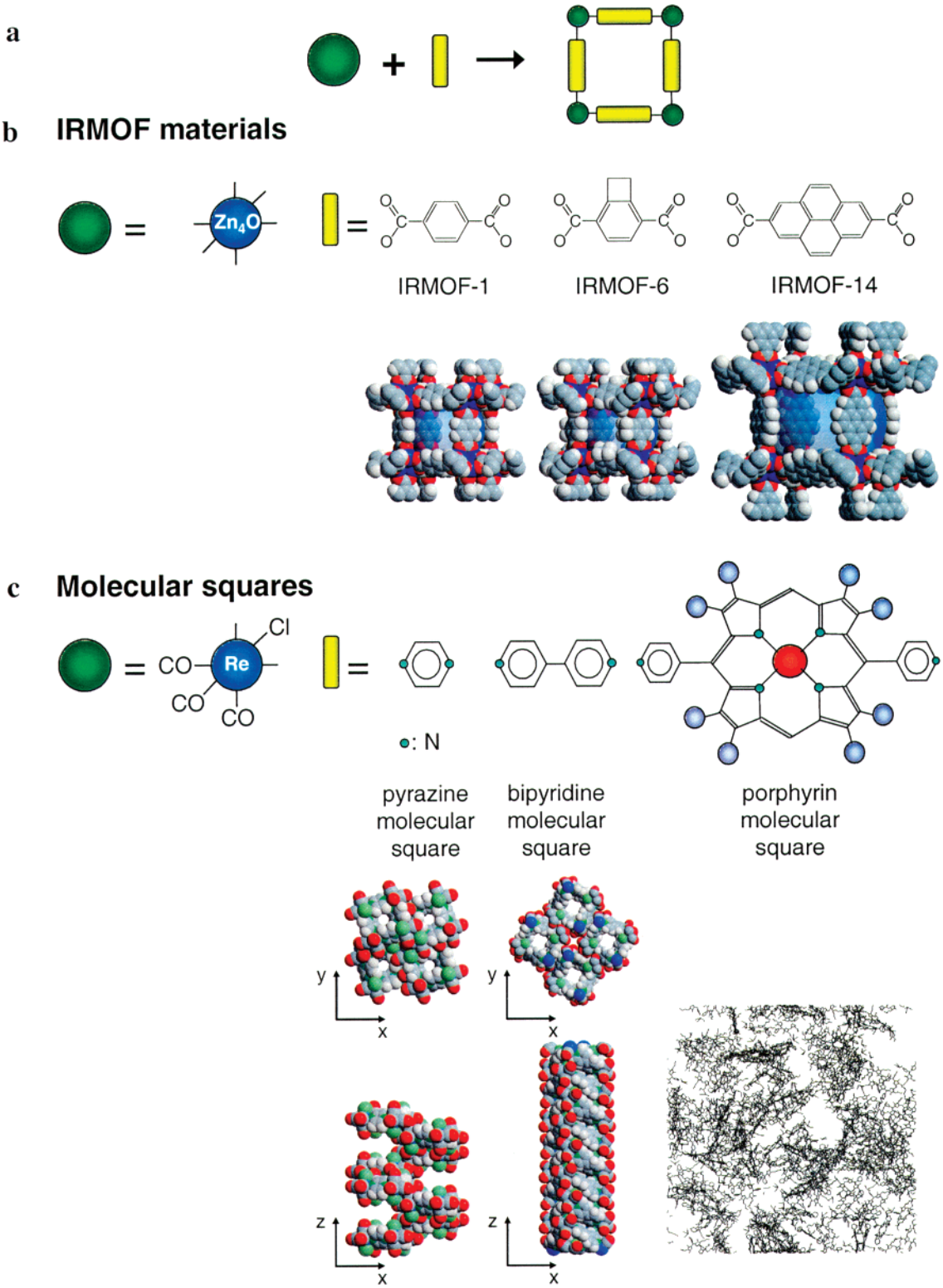

Figure 1. Two examples of ligand-bridged metal−organic materials synthesized in a self-assembly process. (a) Schematic representation of the self-assembly process from corner and bridging units. (b) Building blocks and the resulting three-dimensional frameworks of different IRMOF materials. The empty lines at the ZnO_4 corner units illustrate where the linkers can bind. One complete, larger cavity of each IRMOF framework is shown. The transparent blue spheres were added to demonstrate the size of the cavity and to emphasize the open three-dimensional frameworks. (c) Building blocks of different molecular squares and the resulting structures. The pyrazine and the bipyridine molecular squares form crystalline phases, and a small piece of each crystal is shown from two different orientations. The porphyrin molecular squares are amorphous and were represented in this study by a random packing of individual squares, which is shown at the bottom right of the figure with a stick representation of the packed squares.

amorphous packings of porphyrin and bipyridine molecular squares[11] in this study. Pyrazine molecular squares are arranged helically in the crystal. The space inside the squares themselves is too small to accommodate CH_4 so that adsorption can only take place in the helical channels between the squares (size, 6.14 Å) as shown in Figure 1c.

(11) Sarkisov, L.; Düren, T.; Snurr, R. Q. *Mol. Phys.*, in press.

The puckered bipyridine molecular squares shown in Figure 1c form well-defined channels through the centers of the squares (diameter, 4.58 Å), but spaces between the squares are not accessible to methane molecules. Hypothetical structures of randomly packed individual porphyrin and bipyridine molecular squares were used to mimic amorphous materials (Figure 1c).

Several other commonly studied adsorbents were included for comparison. Silicalite is a microporous zeolite that consists of intersecting straight and zigzag channels (pore diameter, 5.3 Å).[12] Faujasite zeolite has large spherical cavities, with each cavity connected to four others in a tetrahedral arrangement. The cavities have a diameter of 12.5 Å and windows of 7.5 Å.[12] MCM-41 is an ordered mesoporous molecular sieve that consists of hexagonally ordered arrays of long unconnected cylindrical pores with amorphous surfaces and diameters ranging from 15 to 100 Å.[13,14] Carbon nanotubes (CNTs) comprise coaxial tubes of enrolled graphitic sheets with the inner diameter of the tubes in the nanometer range.[15,16] For this simulation study, we used arrays of single-walled carbon nanotubes with varying diameters and interstitial spacings. Note, however, that the interstitial spacing is not a parameter that can be easily controlled experimentally. These carbon nanotube structures are therefore purely hypothetical materials, but they do provide some insight that is useful for designing real materials.

Simulation Details

Equilibrium between the bulk methane phase and the adsorbed phase is modeled with grand canonical Monte Carlo (GCMC) simulations using an atomistic model of methane and the adsorbents. Detailed descriptions of GCMC simulations are given in several references.[17,18] We used our multipurpose simulation code Music[19] with methane−methane and the methane−adsorbent interactions modeled by the Lennard-Jones potential between all pairs of sites. Interactions beyond 12.8 Å were neglected, and the Lorentz−Berthelot mixing rules were used to calculate mixed Lennard-Jones parameters. Methane was represented by the united-atom model, that is, described by a single interaction site. The potential parameters were taken from Goodbody et al.[20] (σ_{CH_4} = 3.73 Å, ϵ_{CH_4}/k_B = 148 K) and were used to describe the methane interactions in all materials. We used an all-atom representation of the adsorbents with the usual simplification that the silicon atoms in the zeolites and MCM-41 were ignored, as their effect on adsorption is small. To describe the interactions with the IRMOF materials and the molecular squares, the all-atom form of the DREIDING potential[21] was used. For the porphyrin squares, the united-atom description was used. For oxygen in silicalite and faujasite, Lennard-Jones parameters were taken from the literature[22] where it was shown that they result in excellent agreement between experimental and simulated methane isotherms in silicalite. Note that we used the pure silica form of faujasite for the simulations. For this paper, we used an MCM-41 with a Barrett−Joyner−Halenda (BJH) diameter of 40.9 Å represented by a single cylindrical pore, for which good quantitative agreement between experimental and simulated methane adsorption was shown before.[23] The arrays of nanotubes consisted of carbon nanotubes in the armchair configuration[16] with varying diameters and interstitial spacing. The single tubes of the first array had a diameter of 13.6 Å and were arranged in a triangular array with a distance of 17 Å between two adjacent tubes[24,25] (denoted here as CNT_i17.0). Furthermore, two arrays with the same interstitial spacing but different pore diameters (10.9 Å (CNT_d10.9) and 15 Å (CNT_d15.0)) and one array that allows methane adsorption in the interstitial spaces (distance between two pores, 20.7 Å; CNT_i20.7) were included in this study. The potential parameters for carbon were taken from Steele.[26] Although these parameters were developed for slit pores, they are commonly used for simulations in carbon nanotubes.[24]

The GCMC simulations were carried out at 298 K with 500 000 equilibration steps and another 500 000 production steps to collect the data at each value of the imposed pressure. The output of such a simulation is the absolute amount adsorbed, that is, the total number of adsorbate molecules present in the pore, whereas experimentally the excess amount adsorbed is measured. The excess number of molecules, n^{ex}, is related to the absolute number of molecules, n^{abs}, by

$$n^{ex} = n^{abs} - V^g\rho^g \tag{1}$$

where V^g is the pore volume of the adsorbent and ρ^g is the molar density of the bulk gas phase calculated with the Peng−Robinson equation of state. V^g is calculated with the second virial coefficient as described in ref 27

$$V^g = \frac{1}{m}\int \exp(-\mathscr{V}(\mathbf{r})/k_BT)\, d\mathbf{r} \tag{2}$$

Here, $\mathscr{V}$ is the fluid−adsorbent interaction of a single helium atom (σ_{He} = 2.58 Å, ϵ_{He}/k_B = 10.22 K),[28] m is the mass of the adsorbent, and T is the temperature. The isosteric heat of adsorption at low loading, Q_{st}, was calculated from[29]

$$Q_{st} = RT - \left(\frac{\partial\langle\mathscr{V}\rangle}{\partial\langle N\rangle}\right)_T \tag{3}$$

where R is the gas constant, $\langle\mathscr{V}\rangle$ is the average potential

(12) Baerlocher, C.; Meier, W. M.; Olson, D. H. *Atlas of Zeolite Framework Types*; Elsevier: Amsterdam, 2001.
(13) Kresge, C. T.; Leonowicz, M. E.; Roth, W. J.; Vartuli, J. C.; Beck, J. S. *Nature* **1992**, *359*, 710.
(14) Beck, J. S.; Vartuli, J. C.; Roth, W. J.; Leonowicz, M. E.; Kresge, C. T.; Schmitt, K. D.; Chu, C. T.-W.; Olsen, D. H.; Sheppard, E. W.; McCullen, S. B.; Higgins, J. B.; Schlenker, J. L. *J. Am. Chem. Soc.* **1992**, *114*, 10834.
(15) Iijima, S. *Nature* **1991**, *354*, 56.
(16) Harris, P. J. F. *Carbon Nanotubes and Related Structures*: *New Materials for the Twenty-First Century*; Cambridge University Press: Cambridge, 1999.
(17) Allen, M. P.; Tildesley, D. J. *Computer Simulations of Liquids*; Clarendon Press: Oxford, 1987.
(18) Frenkel, D.; Smit, B. *Understanding Molecular Simulation*: *From Algorithms to Applications*; Academic Press: San Diego, 2002.
(19) Gupta, A.; Chempath, S.; Sanborn, M. J.; Clark, L. A.; Snurr, R. Q. *Mol. Simul.* **2003**, *29*, 29.
(20) Goodbody, S. J.; Watanabe, K.; MacGowan, D.; Walton, J. P. R. B.; Quirke, N. *J. Chem. Soc., Faraday Trans.* **1991**, *87*, 1952.
(21) Mayo, S. L.; Olafson, B. D.; Goddard, W. A., III *J. Phys. Chem.* **1990**, *94*, 8897.
(22) Du, Z.; Manos, G.; Vlugt, T. J. H.; Smit, B. *AIChE J.* **1998**, *44*, 1756.
(23) Yun, J.-H.; Düren, T.; Keil, F. J.; Seaton, N. A. *Langmuir* **2002**, *18*, 2693.
(24) Stan, G.; Bojan, M. J.; Curtarolo, S.; Gatica, S. M.; Cole, M. W. *Phys. Rev. B* **2000**, *62*, 2173.
(25) Muris, M.; Dupont-Pavlovsky, N.; Bienfait, M.; Zeppenfeld, P. *Surf. Sci.* **2001**, *492*, 67.
(26) Steele, W. A. *The Interaction of Gases with Solid Surfaces*; Pergamon Press: Oxford, 1974.
(27) Myers, A. L.; Monson, P. A. *Langmuir* **2002**, *18*, 10261.
(28) Hirschfelder, J. O.; Curtiss, C. F.; Bird, R. B. *Molecular Theory of Gases and Liquids*; John Wiley: New York, 1964.
(29) Snurr, R. Q.; Bell, A. T.; Theodorou, D. N. *J. Phys. Chem.* **1993**, *97*, 13742.

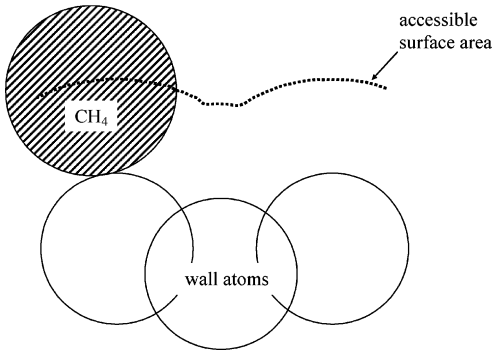

Figure 2. Definition of the accessible surface area.

energy of the adsorbed phase, and $\langle N \rangle$ is the average number of molecules adsorbed.

To characterize the structure of the different adsorbents, we calculated the surface area and the pore size distribution.[30] We used a simple Monte Carlo simulation to get the surface area accessible to methane molecules, S_{acc}, defined by the centers of methane molecules rolling on the surface as shown in Figure 2. Note that the surface area depends on the size of the probe molecule (methane in our case) and is not exactly equivalent to experimentally measured surface areas using nitrogen. Furthermore, we calculated the free volume fraction V_{free}, given by the proportion of the void volume calculated by eq 2 to the total volume of the simulation cell; the porosity, ρ_{free}, defined as the void volume per mass of adsorbent; and the crystalline density, ρ_{crys}.

Results

Figure 3 shows experimental[5] and simulated adsorption isotherms for methane in IRMOF-1 and IRMOF-6 at 298 K. Details of the experimental procedure are given in refs 31 and 32. For both materials, quantitative agreement is observed over nearly the whole pressure range. The average deviation between simulation and experiment is 5.7% for IRMOF-1 and 9.9% for IRMOF-6 with the highest deviations in the low-pressure range where both simulated and experimentally measured values have the largest uncertainties. Similar results were obtained with another standard force field, the UFF force field[33] (7.4% for IRMOF-1 and 9.8% for IRMOF-6), indicating that these results are not very sensitive to the choice of the force field. Because we model only physisorption and not chemisorption, the excellent agreement with the experimental results is a strong indication that physical adsorption is responsible for the high methane uptake in IRMOF materials. In addition, the agreement with experiment using only standard parameters from the literature gives us confidence to use the model in elucidating the features of adsorbents that display high physisorption and to design new IRMOF materials for methane storage using computer simulation.

From the adsorption literature,[34] one expects that the best material to achieve high methane adsorption per mass or volume of adsorbent would have the following properties: *high accessible surface area (S_{acc}), high free volume (V_{free}), low adsorbent framework density (ρ_{crys}), and a strong energetic interaction with the adsorbed methane.* The last feature can be characterized by the isosteric heat of adsorption at low loading (Q_{st}). For simple slit pores, previous theoretical studies[35,36] have shown that the optimal pore diameter is around 8 Å, so that the pores can accommodate two adsorbed layers of methane. (Note however, that studies that include heat and mass transfer effects, which do not play a role in this study, show that a pore diameter of 15−25 Å is desirable.[37]) The challenge with more complicated adsorbent geometries is that the desirable properties listed above are not all necessarily compatible. For example, increasing the free volume may create very wide pores, but the heat of adsorption for molecules in the centers of such wide pores may be close to zero and this space is wasted. On the other hand, the heat of adsorption is higher in smaller pores, but the capacity of such pores may be smaller.

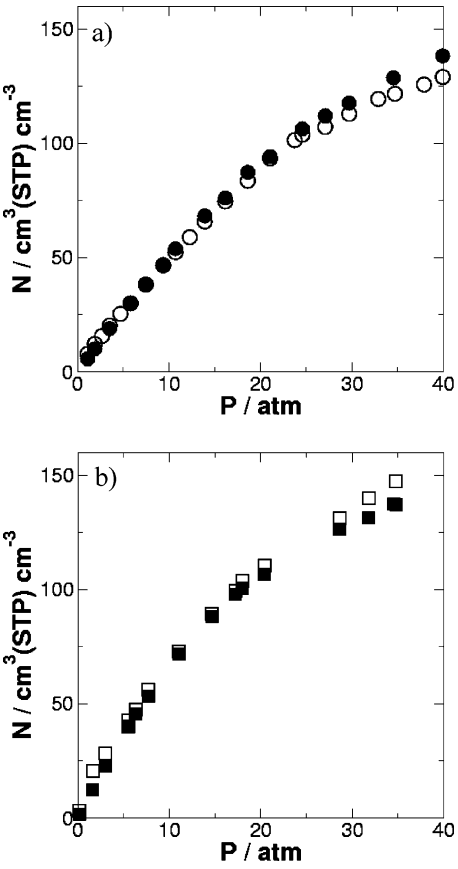

Figure 3. Experimental and simulated methane adsorption isotherms at 298 K: (a) IRMOF-1 and (b) IRMOF-6 (open symbols, experimental results; closed symbols, simulation results).

Table 1 summarizes the important structural characteristics and calculated adsorption properties of all adsorbents considered in this study. As indicated in the last column, concentrations inside the pores are several hundred times higher than in the bulk fluid phase, but some adsorbents are clearly better than others. We now consider which characteristics play the main role in determining methane uptake. We will concentrate on the amount adsorbed per volume or per mass at 35 bar, as this is a primary target for methane storage in vehicular applications.

(30) Gelb, L. D.; Gubbins, K. E. *Langmuir* **1999**, *15*, 305.
(31) Li, H.; Eddaoudi, M.; Groy, T. L.; Yaghi, O. M. *J. Am. Chem. Soc.* **1998**, *120*, 8571.
(32) Eddaoudi, M.; Li, H.; Yaghi, O. M. *J. Am. Chem. Soc.* **2000**, *122*, 1391.
(33) Rappé, A. K.; Casewit, C. J.; Colwell, K. S.; Goddard, W. A., III; Skiff, W. M. *J. Am. Chem. Soc.* **1992**, *114*, 10024.
(34) Ruthven, D. M. *Principles of Adsorption and Adsorption Processes*; VCH: New York, 1984.
(35) Matranga, K. R.; Stella, A.; Myers, A. L.; Glandt, E. D. *Sep. Sci. Technol.* **1992**, *27*, 1825.
(36) Cracknell, R. F.; Gordon, P.; Gubbins, K. E. *J. Phys. Chem.* **1993**, *97*, 494.
(37) Bilóe, S.; Goetz, V.; Guillot, A. *Carbon* **2002**, *40*, 1295.

Table 1. Properties of Adsorbents Investigated

	S_{acc}, m^2/cm^3	S_{acc}, m^2/g	ρ_{crys}, g/cm^3	V_{free}, %	ρ_{free}, cm^3/g	Q_{st}, kJ/mol	$P = 35$ bar amount ads, $cm^3(STP)/cm^3$	$P = 35$ bar amount ads, $cm^3(STP)/g$	$P = 35$ bar uptake/bulk, %
IRMOF-1	2099	3558	0.59	81	1.37	10.6	128.29	217.45	464
IRMOF-6	1966	3025	0.65	77	1.18	12.1	135.46	208.39	517
IRMOF-14	1821	4923	0.37	89	2.38	10.0	100.18	270.77	333
IRMOF-0	2119	1994	1.06	69	0.65	13.3	142.30	134.24	605
IRMOF-991	2171	3179	0.68	80	1.18	9.1	115.12	169.30	421
IRMOF-992	1792	1381	1.30	77	0.59	14.5	167.23	128.84	637
IRMOF-993	1529	1892	0.81	73	0.90	15.5	181.00	224.01	727
pyrazine squares	2004	1318	1.52	48	0.32	14.7	120.91	79.70	723
bipyridine squares	436	248	1.76	24	0.14	21.6	44.20	25.19	526
random porphyrin squares	1939	3526	0.55	76	1.38	16.7	108.73	199.51	422
random bipyridine squares	1884	2369	0.80	67	0.87	14.5	102.22	128.58	434
silicalite	691	399	1.79	29	0.16	19.7	88.00	49.16	898
faujasite	1209	902	1.34	47	0.35	11.3	78.45	58.54	485
MCM-41	551	754	0.73	67	0.92	8.5	41.57	56.95	181
CNT_i17.0	927	719	1.29	51	0.40	17.4	109.24	84.68	628
CNT_i20.7	2551	2804	0.91	80	0.92	14.4	160.79	119.99	997
CNT_d15.0	898	730	1.23	55	0.45	14.1	80.16	59.82	497
CNT_d10.9	726	490	1.48	42	0.28	20.0	27.27	20.35	169

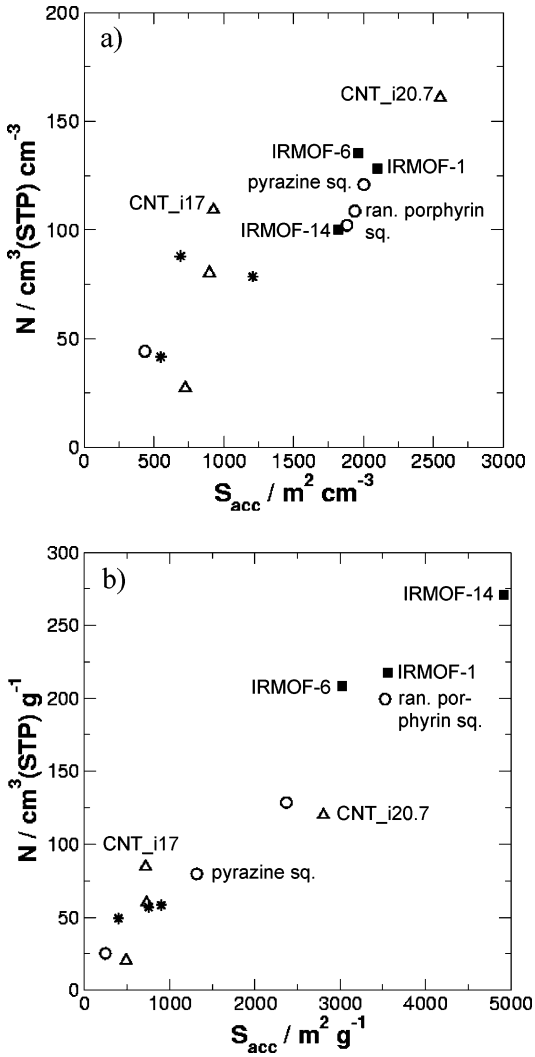

Figure 4. Amount adsorbed at 35 bar as a function of the accessible surface area (a) per volume and (b) per mass (■, IRMOFs; ○, molecular squares; △, CNTs; *, zeolites and MCM-41).

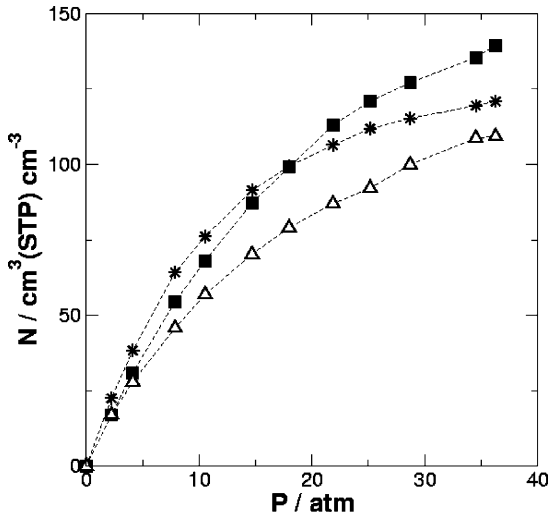

Figure 5. Simulated adsorption isotherms for (■) IRMOF-6, (*) pyrazine molecular squares, and (△) randomly packed porphyrin molecular squares.

Figure 4a,b shows that the amount adsorbed at 35 bar clearly increases with increasing surface area, but a band of data points is observed rather than a single line. The carbon nanotube with a diameter of 13.6 Å and an interstitial spacing of 20.7 Å (CNT_i20.7, see Simulation Details) shows the highest surface area and the highest uptake per volume. This interstitial spacing was artificially constructed to allow for exactly one row of methane molecules between all nanotubes, although this spacing would be extremely difficult to produce experimentally. If the interstitial spacing is changed to 17 Å (CNT_i17), there is considerably less adsorption because methane does not fit between tubes. CNT_i20.7 shows such a high methane uptake because methane molecules can adsorb at both sides of the CNT surfaces. This "double duty" is also true of the linkers of the IRMOF materials, so that IRMOF-1 and IRMOF-6 show the second and third highest uptake of methane per volume. In comparing IRMOF-1 and IRMOF-6, one may expect that the latter should have a higher surface area because of the extra cyclic group on each linker (Figure 1). However, the additional surface groups create excluded areas close to the corners of the IRMOF cages that become inaccessible to methane molecules, thus reducing the accessible surface area for IRMOF-6 as indicated in Figure 4 and Table 1.

High free volume and low framework density are related features of a material. If the amount adsorbed per mass of adsorbent is considered, as in Figure 4b, the IRMOF materials, especially IRMOF-14, show the highest uptake

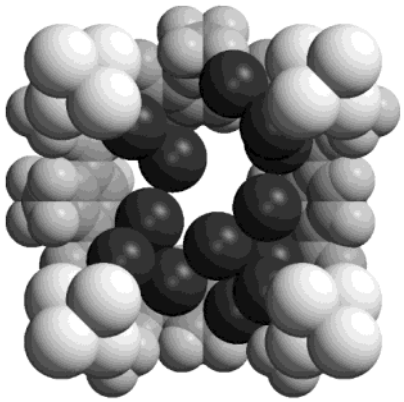

Figure 6. Snapshot of methane molecules (dark gray spheres) adsorbed in IRMOF-6 (gray framework) at 35 bar. The number of molecules shown corresponds to the average loading in a larger cavity. The four linkers connecting the corners at the front of the figure (white spheres) are removed for clarity.

because of their low framework density. Crystalline bipyridine molecular squares, the zeolites, and MCM-41 do not display surface areas as high as those of the IRMOFs on a volumetric or mass basis, because their framework densities are higher and their free volumes are lower (see Table 1). They also do not adsorb nearly as much methane at 35 bar. The crystalline pyrazine square has a high surface area on a volumetric basis, but its high framework density and low free volume lead to a lower relative surface area and a lower amount adsorbed when considered on a mass basis (Figure 4b).

Another way the free volume can affect the amount adsorbed is shown in Figure 5. At the pressure of interest, 35 bar, the isotherm for the pyrazine square is already approaching saturation, that is, the free volume is almost filled with methane. The isotherm for IRMOF-6, on the other hand, is still rising at 35 bar (Figure 5). Thus, even though both materials have fairly similar surface areas on a volumetric basis, the loading in IRMOF-6 is higher (135 vs 121 in volume units, see Table 1). Figure 6 shows a snapshot of the IRMOF-6 system at 35 bar. It shows that the molecules prefer to be near the walls, but there is still plenty of open space in the middle of the cage.

Next, we consider the effect of the energetic interactions on the loading. Comparing IRMOF-1 and IRMOF-6, one sees in Table 1 that the additional atoms on the linkers of IRMOF-6 increase the low-loading heat of adsorption by providing additional interaction sites. This leads to an increased amount adsorbed at 35 bar in IRMOF-6, even though IRMOF-1 has a higher accessible surface area (properties considered on a volumetric basis).

A final consideration is the distribution of pore sizes. As mentioned above, large pores do not adsorb much methane as their interaction potential is too weak. The calculated pore size distribution for the randomly packed molecular squares shows a wide range of pore sizes. Thus, the isotherm for the random porphyrin square (Figure 5) lies considerably below that of IRMOF-6, although the two materials have similar surface areas and free volumes.

We may conclude that the ideal material should have a large accessible surface area. In addition, high free volume (V_{free}), low framework density (ρ_{crys}), and strong energetic interactions with the adsorbed methane are also desired, but changing the pore size to improve one of these may worsen the others in a complex manner. GCMC simulations allow us to evaluate complex material topologies even if simple rules of thumb are unavailable or in conflict.

Keeping the complex interplay of the different factors in mind, we tested several new, not yet synthesized

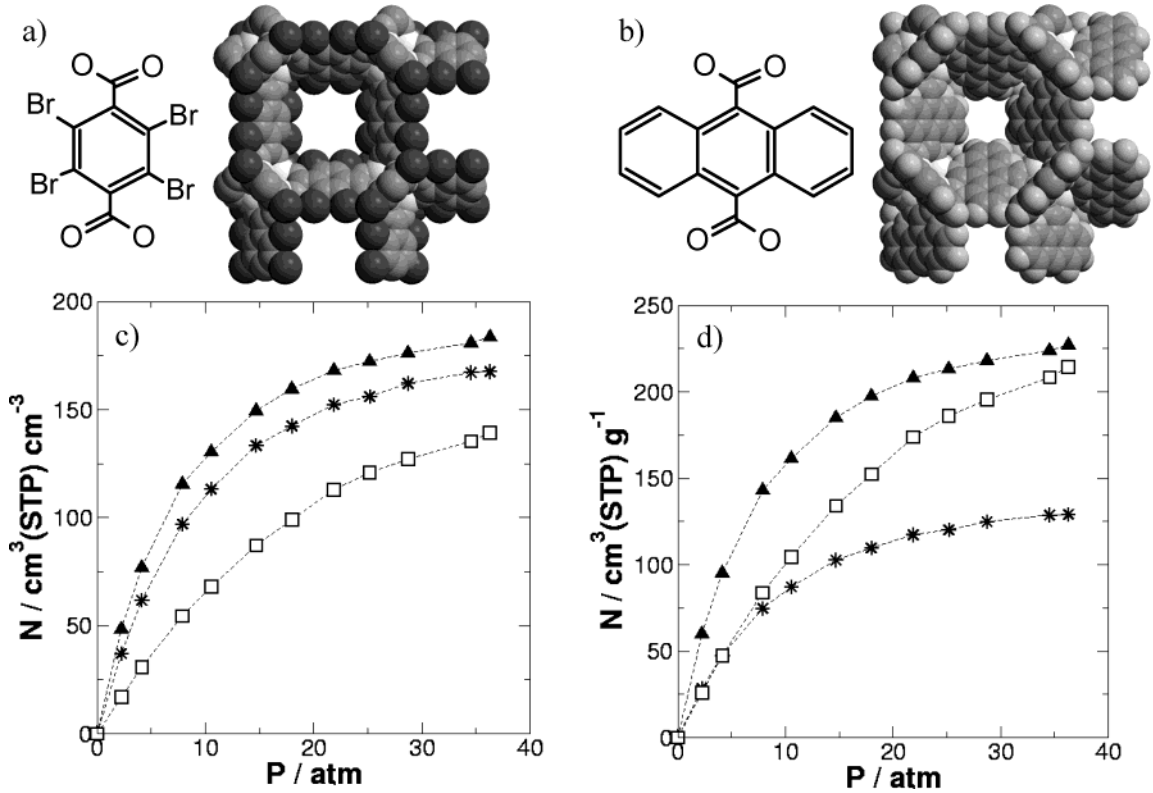

Figure 7. Molecularly designed IRMOF materials and the predicted adsorption isotherms: (a) IRMOF-992, which uses 1,4-tetrabromobenzenedicarboxylate as the linker molecule; (b) IRMOF-993, which uses 9,10-anthracenedicarboxylate; (c) adsorption isotherms as amount adsorbed per volume; (d) adsorption isotherms as amount adsorbed per mass adsorbent (*, IRMOF-992; ▲, IRMOF-993; □, IRMOF-6).

structures for their potential use in methane storage, building on the idea that the IRMOF materials are isorecticular[5] (i.e., they have the same network topology). Since a wide variety of similar IRMOFs have already been synthesized using different linkers,[5] we have some reason to hypothesize that the proposed materials may be synthetically accessible and stable. We assigned the newly designed IRMOF materials numbers starting from 991 to distinguish them from already synthesized materials. First, we designed two smaller IRMOF materials to come closer to the ideal pore diameter of about 8 Å:[35,36] one without any additional linker molecules (IRMOF-0; cavity diameter, 8.5 Å/9.7 Å) and one with ethinedicarboxylate as the linker (IRMOF-991; cavity diameter, 11.7 Å). IRMOF-0 showed a slightly higher uptake of CH_4 compared to IRMOF-6 at 35 bar (142.3 cm^3(STP)/cm^3), but IRMOF-991 was considerably worse (115.1 cm^3(STP)/cm^3), as the number of interaction sites is reduced by 48 C atoms per cavity.

A more successful approach is to use IRMOF-1 as the starting point and to replace or add atoms in the linker molecules. Replacing the hydrogen atoms by bromine atoms (i.e., using 1,4-tetrabromobenzenedicarboxylate as linker molecules, see IRMOF-992, Figure 7a) introduces stronger interaction sites. The resulting adsorption isotherm presented in Figure 7c indeed shows a higher uptake of methane per volume of adsorbent over the whole pressure range, with an isosteric heat of adsorption at low loading of 14.47 kJ/mol. Yet, because of the higher crystalline density ($\rho_{crys} = 1.30$ g/cm^3) the amount adsorbed per mass of adsorbent is lower than for the other IRMOF materials as shown in Figure 7d. Using 9,10-anthracenedicarboxylate as linker molecules (IRMOF-993, Figure 7b) results in a material with a crystalline density of 0.81 g/cm^3. Because of the large size and the alternating orientation of the linker molecules, the size of the smaller cavities ($d = 6.3$ Å) and the accessible surface area ($S_{acc} = 1529$ m^2/cm^3) are significantly reduced. Nevertheless, the amount adsorbed is higher over the whole pressure range as shown in Figure 7c. At 35 bar, IRMOF-993 even exceeds the revised target value of 180 v/v (181 v/v). The reason for this is the significantly increased number of interaction sites ($Q_{st} = 15.48$ kJ/mol vs 12.1 kJ/mol for IRMOF-6) and the pore size of the small cavities which is close to the optimal value. As the crystalline density of IRMOF-993 is close to the density of other IRMOF materials, the performance is also excellent if the amount adsorbed per mass adsorbent is considered (Figure 7d).

Conclusions

In this paper, the applicability of different materials for methane storage was investigated. Specifically, using molecular simulations we examined the extraordinary capacity of IRMOF materials for methane adsorption. By using a standard force field without fitting any parameters, quantitative agreement between the simulated and experimental adsorption isotherms was achieved for IRMOF-1 and IRMOF-6. This strongly suggests that the high methane uptake observed experimentally in IRMOF-6 (155 cm^3(STP)/cm^3 at 35 bar) is due to physical adsorption. By comparing adsorption in different materials (three IRMOF materials, four molecular squares, two zeolites, MCM-41, and four carbon nanotubes) and calculating different properties that characterize these materials, we were able to identify the complex interplay of factors that influence adsorption. An ideal material for CH_4 adsorption should have not only a large accessible surface area but also a high free volume, a low framework density, and strong energetic interactions between the framework and the methane molecules. Yet, changing one of these parameters might worsen the others and therefore decrease the amount adsorbed. IRMOF-6 shows such a high performance in methane adsorption because it shows all of the properties mentioned above. Because of their low crystalline density, IRMOF materials seem to be a good compromise if the amount adsorbed per volume and the amount adsorbed per mass of the adsorbent must both be taken into account. Based on this analysis, we also proposed new, not yet synthesized IRMOF materials that are predicted to show substantially higher uptake of methane than IRMOF-6. The simulations show that by using 1,4-tetrabromobenzenedicarboxylate and 9,10-anthracenedicarboxylate as linker molecules, the amount adsorbed per volume can be increased by 23% and 36%, respectively. The quantitative agreement between simulations and experiments for IRMOF-1 and IRMOF-6 provides support for the power of the computational method. Thus, this study underlines the usefulness of GCMC simulations as a screening tool to identify new candidates for methane storage and other adsorption applications and to guide the design of new materials. In addition, the results open new possibilities for the use of adsorbed natural gas as an alternative fuel.

Acknowledgment. The authors thank the U.S. Department of Energy and the Alexander von Humboldt Foundation for financial support.

Supporting Information Available: Values for the experimental and simulated adsorption isotherms shown in Figure 3; values for the simulated adsorption isotherms shown in Figure 5; values for the simulated adsorption isotherms shown in Figure 7. This material is available free of charge via the Internet at http://pubs.acs.org.

LA0355500